BM-D-19-00099

Biaxial Biomechanical Properties of the Nonpregnant Murine Cervix and Uterus

Conway, Cassandra K.
Department of Biomedical Engineering, Tulane University
6823 St. Charles Ave, New Orleans, LA 70118 USA
cconway2@tulane.edu

Qureshi, Hamna J.
Weldon School of Biomedical Engineering, Purdue University
206 S. Martin Jischke Drive, West Lafayette, IN 47907
hjquresh@purdue.edu

Morris, Victoria L.
Department of Biomedical Engineering, Tulane University
6823 St. Charles Ave, New Orleans, LA 70118 USA
Victoria.Morris@uth.tmc.edu

Danso, Elvis K.
Department of Biomedical Engineering, Tulane University
6823 St. Charles Ave, New Orleans, LA 70118 USA
edanso@tulane.edu

Desrosiers, Laurephile
Department of Female Pelvic Medicine & Reconstructive Surgery, Ochsner Clinical School
1514 Jefferson Highway, New Orleans, LA 70121
laurephile.desrosiers@ochsner.org

Knoepp, Leise R.
Department of Female Pelvic Medicine & Reconstructive Surgery, Ochsner Clinical School
1514 Jefferson Highway, New Orleans, LA 70121
lknoepp@ochsner.org

Goergen, Craig J.
Weldon School of Biomedical Engineering, Purdue University
206 S. Martin Jischke Drive, West Lafayette, IN 47907
cgoergen@purdue.edu

Miller, Kristin S.
Department of Biomedical Engineering, Tulane University
6823 St. Charles Ave, New Orleans, LA 70118 USA
(504) 988-9324
kmille11@tulane.edu

Keywords: Biaxial testing; Biomechanics; Structure-function; Murine; Uterus; Cervix; Women's health

ABSTRACT:

From a biomechanical perspective, female reproductive health is an understudied area of research. There is an incomplete understanding of the complex function and interaction between the cervix and uterus. This, in part, is due to the limited research into multiaxial biomechanical functions and geometry of these organs. Knowledge of the biomechanical function and interaction between these organs may elucidate etiologies of conditions such as preterm birth. Therefore, the objective of this study was to quantify the multiaxial biomechanical properties of the murine cervix and uterus using a biaxial testing set-up. To accomplish this, an inflation-extension testing protocol (n=15) was leveraged to quantify biaxial biomechanical properties while preserving native matrix interactions and geometry. Ultrasound imaging and histology (n=10) were performed to evaluate regional geometry and microstructure, respectively. Histological analysis identified a statistically significant greater collagen content and significantly smaller smooth muscle content in the cervix as compared to the uterus. No statistically significant differences in elastic fibers were identified. Analysis of bilinear fits revealed a significantly stiffer response from the circumferentially orientated ECM fibers compared to axially orientated fibers in both organs. Bilinear fits and a two-fiber family constitutive model showed that the cervix was significantly less distensible than the uterus. We submit that the regional biaxial information reported in this study aids in establishing an appropriate reference configuration for mathematical models of the uterine-cervical complex. Thus, may aid future work to elucidate the biomechanical mechanisms leading to cervical or uterine conditions.

INTRODUCTION

Recent work on the female pelvic floor emphasized the importance of quantifying biaxial properties to improve basic understanding of physiological function and pathologies of the female reproductive tract (Baah-Dwomoh et al. 2016, Myers et al. 2015, Becker and De Vita 2015, Manoogian et al. 2008). For example, cervical insufficiency or pelvic organ prolapse have an unknown etiologies, however, remodeling of microstructure and a dynamic loading environment play a significant role (Leppert et al. 1987, Yoshida et al. 2014a, Luo et al. 2015). Fluctuations in geometry and microstructural composition dictate changes in biomechanical properties and organ function in response to physiologic changes such as cyclical hormones, pregnancy, and post-partum recovery (Yoshida et al. 2014a, Akins et al. 2011, Ferland, Darios and Watts 2015).

Two organs of interest, the cervix and uterus, have complex functions, geometry, and microstructure. Previous work quantified the microstructure and mechanical response of the cervix and uterus in human (Danforth 1947, Rorie and Newton 1967, Leppert, Cerreta and Mandl 1986, Conrad et al. 1966, Pearsall and Roberts 1978), rat (Harkness and Moralee 1956, Harkness and Harkness 1959, Sharrow et al. 1989), and mouse (Leppi 1964, Loeb, Suntzeff and Burns 1938, Yoshida et al. 2014b). To date, cervical and uterine biomechanical properties are primarily determined uniaxially (Harkness and Harkness 1961, Conrad et al. 1966, Pearsall and Roberts 1978, Myers et al. 2010, Yoshida et al. 2014a, Barnum et al. 2017). However, the cervix and uterus are loaded multiaxially within the body, resulting in changes in luminal diameter and length with the menstrual cycle and alterations in intra-abdominal pressure (Bulletti et al. 2000, Harkness and Harkness 1959).

Planar uniaxial or biaxial testing require sample preparation that alters the shape of the tissue and does not preserve the matrix-cell interactions. Biaxial inflation-extension protocols, contrastingly, preserve tissue geometry, ECM interactions, and permit evaluation of tissue anisotropy within an estimated physiologic axial extension over a physiologic range of pressures (Van Loon 1976, Gleason et al. 2004, Amin, Le and Wagenseil 2012, Bersi et al. 2014). This technique, to date, has not been used for the murine cervix or uterus.

A need remains to investigate the biomechanical properties of the organs to better understand the axial-circumferential interactions within the organs and to investigate the organs as a continuous structure. Maintaining the organs' native geometry and matrix interactions enables quantification of the gradient of mechanical properties through the reproductive tract. Quantifying the geometry, microstructure, and biomechanics of each organ is necessary to develop accurate models to determine the causes of reproductive pathologies (Fernandez et al. 2016, Westervelt et al. 2017, Lepage et al. 2015). Therefore, the objective of this study was to quantify the regional biaxial biomechanical properties, geometry, and microstructure of the murine cervix and uterus.

2. MATERIALS AND METHODS

2.1 Animal Care

The use of animals were conducted with the approval of the Institutional Animal Care and Use Committee (IACUC) at Tulane University and Purdue University. A total of n=16 (10 from Purdue University and 6 from Tulane University) virgin female C57BL/6J mice at 4-6 months of age were utilized for the study (Jackson Laboratory, Bar Harbor, ME). Mice were housed in a 12-hour light/dark cycle on a normal diet. Estrous cycle phase

was monitored and determined visually. All experiments were performed on female mice at estrus (Byers et al. 2012).

2.2 Ultrasound imaging of in vivo geometry

Reproductive tracts from 10 female C57BL/6J mice between 4-6 months of age were imaged using a Vevo2100 ultrasound system (FUJIFILM VisualSonics, Inc, Toronto, ON, Canada) (Fig. 3). Utilizing a 22-55MHz transducer with a central frequency of 40MHz (MS550D) and a linear step motor, 2D short axis B-mode slices were taken with a step size of 0.19mm along the length of the reproductive system and compiled into 3D representations (Fig. 4).

Measurements of thickness and diameter were taken at the base of the uterine horn and the mid-cervix (Fig. 5A, 5B). Animals were euthanized at estrus via CO_2 inhalation, frozen at -20°C, shipped to Tulane University, and stored at -20°C. Noting that prior research determined there are no significant effects of a freeze-thaw cycle on the passive mechanical behavior of the cervix (Yoshida et al. 2016).

2.3 Sample collection and preparation

Stain markings were placed every 3mm along the exposed reproductive tract with India Ink (Dick Blick Art Materials, Galesburg, IL) (Robison et al. 2017). Markings were placed immediately inferior to the ovary, centered on the cervix, and immediately superior to the vaginal introitus. During excision, the reproductive organs retracted from their original positions. For repeatability, singular cuts were made superior to the mark above the central cervix mark and inferior to the mark below to the central mark for a known *in situ* length of 6mm as an initial approximation of physiologic length (Fig. 1A) (Robison et al. 2017).

Samples were bathed in Hank's balanced saline solution (HBSS) at 4°C, excess vaginal tissue removed from the exterior of the external os, and one uterine horn was randomly selected for mechanical assessment while the secondary uterine horn was ligated with 6-0 silk suture (Fig. 1B,C). Specimens were cannulated at the uterine horn and external os within a myograph inflation-extension device (Danish MyoTechnologies, Aarhus, Denmark; Fig. 1C) with 6-0 silk suture.

Cannulated specimens were stretched to an estimated unloaded length visually determined as the length wherein the organ was not in compression or tension. A Nikon Eclipse TS100 inverted microscope (Nikon®, Melville, NY, U.S.A.) optically measured unloaded *ex situ* diameters at the uterine and cervical regions and digital calipers measured *ex situ* lengths. Samples were maintained at 37°C in HBSS.

2.4 Biomechanical testing

Utero-cervical complexes from Purdue (n=10) and Tulane (n=6) were utilized for extension-inflation testing. Extension-inflation testing permits evaluation of changes in organ diameter in response to variations in intraluminal pressure (pressure-inflation tests) and a controlled length to simulate multiaxial loading within the body (Bulletti et al. 2000, Harkness and Harkness 1959). Extension-inflation testing permits measuring changes in axial force and organ diameter while increasing the organ's length and maintaining a constant intra-luminal pressure (force-elongation tests).

Prior studies show that the measurement of organ mechanical properties is more consistent, repeatable, and mathematically interpretable following preconditioning (Fung, Fronek and Patitucci 1979). Preconditioning provides organs with a "memory" of applied loads and minimizes any permanent (plastic) deformations or loss of energy during

mechanical testing (Fung et al. 1979). The pressure-inflation preconditioning consisted of five cycles performed over a physiologic range of pressures (P=0 to 200mmHg) (Fig. 2B) (Lumsden and Baird 1985, Humphrey 2002, Milsom, Andersch and Sundell 1988). This was followed by five cycles of force-elongation preconditioning at a constant pressure of 67mmHg (1/3 of maximum physiologic pressure) up to 10% above the unloaded length.

An estimated physiologic length was approximated utilizing the assumption that minimal changes in force occur over a range of pressures at the *in vivo* length to conserve energy (Van Loon 1976). The specimen was stretched above the unloaded length to the known *in situ* length (6mm). The organs was subsequently stretched or compressed around the estimated value until the force remained near constant over a range of pressures (Fig. 2).

Subsequently, the organs are subjected three cycles of increasing pressure (P=0-200 mmHg) at static lengths ±2% estimated physiologic lengths (Fig. 2) within a physiologic range above and below the physiologic length determined previously. Cyclically pressurizing the organs at set lengths permits quantification of the mechanical response of the organ throughout a range of physiologic changes.

Force-elongation cycles are performed in which pressure (P = 10, 67, 133, and 200mmHg) is held constant and the length of the organs is cycled through the physiologic range of organ lengths (±2% estimated physiologic lengths). Assuming that organs have a preferred length to conserve force over a range of pressures, the force-elongation protocol confirms the estimated physiologic length at the intersection point of the force to axial stretch ratio, λ_z (Van Loon 1976, Amin et al. 2012).

2.5 Thickness and volume calculation

Following biomechanical testing, 0.5mm thick rings were isolated from the mid-region of the cervix and uterus and imaged with a Moticam 580 HD Digital Camera and Motic Images software (Motic® Richmond, British Columbia). For data analysis of 4 samples, an averaged data set of thickness values (626±22.9 μm for the cervix and 690 ±19.2 μm for the uterus) was utilized. A custom MATLAB code calculated unloaded wall thickness from the ring images (Bersi et al. 2014, Ferruzzi, Bersi and Humphrey 2013).

Assuming a simplified geometry (hollow cylinder), the unloaded cervical and uterine volumes (V) were determined using equation:

$$V=\pi L(R_o^2-R_i^2)\,, \tag{1}$$

where L is the unloaded length and R_o and R_i are the undeformed outer and inner radii, respectively.

2.6 Histology

Cervical and uterine rings 0.5mm thick (n=10) were isolated, fixed in 10% formalin solution for 24 hours, embedded in paraffin wax, and cut into 4μm serial sections. The sections were then stained with Hart's elastic stain, Picrosirius Red (PSR), and Masson's Trichrome (MT). Images were subsequently taken using an Olympus BX51 microscope, an Olympus DP27 Digital Camera, and cellSens™ software (Olympus Corporation, Center Valley, PA, U.S.A.) at 4x and 10x magnification.

All samples were analyzed at 4x magnification. A custom MATLAB code determined ratios comparing large to small diameter collagen fibers assuming that red and orange pixel area fractions associated to large diameter collagen fibers and yellow and green pixel area fractions associated to small diameter collagen fibers (Bersi et al. 2012).

Color deconvolution, an open source plug-in for ImageJ software (National Institutes of Health, Bethesda, MD, U.S.A.) (Ruifrok and Johnston 2001, Rasband 1997-2016), and an open-source GNU image manipulation program (GIMP), were leveraged to determine smooth muscle cell and collagen area fractions (Garipcan et al. 2011, Sparavigna 2014, Capone et al. 2018). Within GIMP the outer and inner ring were selected to diminish background noise. Using a histogram feature within the software, pixels over a range of intensities were chosen to represent the ECM contents and divided out from the total pixels for a calculation of area fraction. For quantifying elastic fiber area fractions, the GIMP select by color tool was utilized to isolate elastic fibers from the section.

2.7 Data analysis

Although the cervix and uterus are thick-walled organs and 3D modeling is necessary to completely describe the organ response, there is limited basic science information on the heterogeneity of the organs' walls. Thus, cervical and uterine geometry was simplified to a thin-walled hollow cylinder assessed in 2D. Additionally, the cervix and uterus were assumed to demonstrate a nonlinear and pseudoelastic biomechanical behavior (Liao et al. 2014, Myers et al. 2010).

Using the initial point data from the -2% estimated physiologic length test as the reference configuration, pressure-diameter data was used to calculate circumferential (σ_θ) and axial (σ_z) Cauchy stresses (Ferruzzi et al. 2013) at each location using equations:

$$\sigma_\theta = \frac{Pa}{h}, \tag{2}$$

and

$$\sigma_z = \frac{F_t + \pi a^2 P}{\pi h(2a+h)}, \tag{3}$$

where P is intraluminal pressure, a is the deformed inner radius, h is the deformed thickness, and F_t is the force from the axial force transducer.

Pressure-diameter data was used to calculate the circumferential and axial stretch ratios which were determined via (Ferruzzi et al. 2013):

$$\lambda_\theta = r_{mid}/R_{mid}, \quad (4)$$

and

$$\lambda_z = l/L, \quad (5)$$

where r_{mid} and R_{mid} represent the loaded and unloaded mid-wall radii and l and L represent the loaded and unloaded axial lengths, respectively.

Bilinear curve fits, an application of linear interpolation, were applied along the two major components of the stress-stretch curve: the toe-region (the lower non-linear region) and the linear region of the stress-stretch data to quantify moduli for each pressure-diameter test (Supplemental 1) (Lake et al. 2009, Robison et al. 2017).

2.8 Constitutive modeling

A pilot study determined an appropriate microstructurally-motivated functional form of a stored energy function (SEF) for the cervix and uterus. The 2D two-fiber family model with a neo-Hookean term (2D 2FF+NH) was employed. The 3D three-fiber family model, previously used to describe human cervical material properties (Liao et al. 2014), was not used as it was over-parameterized for the murine data (Yin, Chew and Zeger 1986). Yin *et al.* described over-parameterization as the calculated determinant of the correlation matrix, $\mathbf{R}<10^{-4}$. Data from the 2% below estimated physiologic stretch were excluded from data analysis as the axial force measured indicated imminent bending or buckling of the organs as described previously (Collins et al. 2012).

The SEF, W, of the 2D 2FF+NH microstructural model utilizes an isotropic term assumed to represent the elastin-dominated ground matrix with a neo-Hookean behavior and an anisotropic collagen-dominated term representing two diagonal fiber directions, measured relative to the axial direction and symmetric about the long axis with an assumed Fung-type exponential (Holzapfel, Gasser and Ogden 2000):

$$W(\mathbf{C}, \mathrm{M}^k) = \frac{c}{2}(I_C - 3) + \sum_k \frac{c_1^k}{2c_2^k} * \exp\left(c_2^k\left((\lambda_k^2) - 1\right)^2\right), \quad (6)$$

where c and c_1 are material parameters that have units of kPa and c_2 is a dimensionless material parameter, $\mathbf{C} = \mathbf{F}^T \cdot \mathbf{F}$ is the right Cauchy-Green tensor, $\mathrm{M}^k = [0, \sin\alpha_0^k, \cos\alpha_0^k]$ is the fiber orientation unit vector where α_0^k was set at $\alpha_0^k = \pm\alpha_0$ for diagonal, symmetric alignment, I_C is the first invariant of the right Cauchy Green tensor, $I_C = tr\mathbf{C} = \lambda_\theta^2 + \lambda_z^2 + \lambda_r^2$, where $\lambda_r = 1/\lambda_\theta\lambda_z$, and $\lambda_k^2 = \mathrm{M}^k \cdot \mathbf{C}\mathrm{M}^k$ is the fourth invariant which defines the stretch experienced by the kth fiber family. Theoretical Cauchy stresses were determined from (Humphrey 2002):

$$\boldsymbol{t} = -p\mathbf{I} + \frac{2}{J}\mathbf{F} \cdot \frac{\partial \mathrm{W}}{\partial \mathbf{C}} \cdot \mathbf{F}^T, \quad (7)$$

where p is the Lagrange multiplier, $\mathbf{F}$ is the deformation tensor, and $J = det\mathbf{F}$.

Equation 7 and non-linear regression were utilized via MATLAB to minimize error between the theoretical and experimental data, determine best-fit parameters, and ensure unique parameters for the 2D 2FF+NH model using the following objective function (Ferruzzi et al. 2013):

$$e = \sum_{i=1}^{N}\left[\left(\frac{P_{th} - P_{exp}}{\bar{P}_{exp}}\right)_i^2 + \left(\frac{F_{th} - F_{exp}}{\bar{F}_{exp}}\right)_i^2\right], \quad (8)$$

where F_{th} and F_{exp} are theoretical and experimental forces, P_{th} and P_{exp} are the theoretical and experimental intraluminal pressures, $\bar{P}_{exp}$ is the mean experimental pressure, and $\bar{F}_{exp}$ is the mean experimental force (Ferruzzi et al. 2013).

2.9 Statistical analysis

All data within the study are presented as mean±standard error of the mean (SEM). One sample was removed due to a disruption in tracking the outer diameter resulting in a total of 15 samples compared for mechanical testing. Biomechanical parameters from bilinear curve fits were analyzed using a two-way repeated measures ANOVA (location, axial coupling), followed by paired Student's t-tests with Bonferroni corrections when appropriate (p<0.05). A paired t-test was used to compare the material parameters, geometries, and area fractions of ECM constituents at the cervix and uterine horn. A Pearson's correlation analysis was performed directly comparing histological area fractions and material parameters from the same sample for both organs.

3. RESULTS

3.1 Bilinear Fits

All parameters for the bilinear fit response are reported in Table 1. The two-way repeated measures ANOVA for $\lambda_\theta \, vs \, \sigma_\theta$ revealed a significantly larger toe-region (p<0.005) and linear-region (p<0.001) moduli for the cervix, as compared to the uterus (Table 1, Fig. 6). The uterus demonstrated increased circumferential stretch (p<0.001) at the transition point between the toe- and linear-regions, as compared to the cervix (Table 1, Fig. 6). For $\lambda_\theta \, vs \, \sigma_z$, the circumferential stretch at the transition point increased significantly (p<0.001) for the uterus compared to the cervix.

The cervix, however, exhibited significantly higher toe (p<0.01) and linear-region (p<0.001) elastic moduli compared to the uterus (Table 1). Comparisons of σ_θ against and σ_z at the same λ_θ indicated a significantly larger (p<0.001) stress value and greater (p<0.001) toe- and linear-regions elastic moduli within the circumferential direction within the cervix. The uterus demonstrated a significantly larger circumferential stress (p<0.05), toe-region modulus (p<0.005), and greater linear-region modulus (p<0.001) in the circumferential direction (Table 1, Fig. 6).

3.2 Material Parameters

The constitutive model described the biomechanical response of the cervix (RMSE=0.30±0.03) and uterus (RMSE=0.28±0.02) reasonably well (Fig. 7, Table 2, 3) (Holzapfel et al. 2000). The neo-Hookean parameter c, the c_1 stress-like parameter, and the c_2 parameter were significantly larger (p<0.05) for the cervix compared to the uterus (Table 2, 3). Fiber angles between the two locations were significantly different (p<0.001), with the cervix and uterus having average fiber angles of 51.5±2.00° and 45.9±1.91°, respectively (Table 2, 3).

3.3 Structure

Paired t-tests performed between the cervical and uterine ultrasound measurements of the *in vivo* thickness and diameter resulted in a significant increase (p<0.05) in both geometric parameters at the cervix (Fig. 5). Histology demonstrated a significant (p<0.005) increase in collagen content for the cervix (75.6±4.49%) in comparison to the uterus (69.6±5.23%) (Fig. 8). PSR analysis revealed a significantly (p<0.001) greater amount of large diameter collagen fibers in comparison to the amount of small diameter fibers at both locations. Further, analysis detected a greater content of larger diameter fibers within the

cervix with an average diameter ratio of 7.47±2.94% compared to 6.12±1.17% in the uterus. The area fraction of the smooth muscle within the uterus was significantly greater (p<0.001) (uterus: 18.4±1.55% vs. cervix: 15.7±3.90%), however, elastic fiber was not significantly different (uterus: 3.63±1.16% vs. cervix: 3.32±0.57%) (Fig. 8). The Pearson's correlation identified no correlation between the collagen content within the cervix and uterus and the material parameters c_1 and c_2.

4. DISCUSSION

In this study, the biaxial material parameters of the cervix and uterus were quantified while preserving native organ structure and matrix interactions (Ferruzzi et al. 2013, Gleason et al. 2004, Amin et al. 2012). The constitutive model used herein identified significantly larger c_1 and c_2 parameters in the cervix compared to the uterus. Additionally, the bilinear fits performed on the stress-stretch curves demonstrated larger linear modulus in both the axial and circumferential directions at the cervix compared to the uterus (Fig. 6). A higher collagen content was identified in the cervix suggesting that the higher collagen content contributes to the decreased distensibility noted in the cervix.

Further, differences in collagen fiber diameter, type I:III composition, organization, and undulation may contribute to the observed regional differences in mechanical properties along the reproductive tract (Capone et al. 2018). Towards this end, a significantly greater amount of large diameter collagen fibrils identified in the cervix may also contribute to the increased collagen model parameters and decreased distensibility. A greater circumferential bias in the collagen fiber alignment in the cervix compared to the uterus, indicated by the larger fiber angle parameter,α, confirms increased resistance to load in the circumferential direction compared to the axial direction.

Clinically, greater resistance to circumferential loading of the cervix and reduced axial resistance correspond with shortening of the cervix in cases of cervical insufficiency (Leppert et al. 1987, Myers et al. 2010). Interestingly, a uniaxial study found a stiffer longitudinal direction within the vagina as compared to the circumferential direction within the cervix and uterus (Peña et al. 2011). However, the uniaxial experiments were performed at greater loads and the organs may have a different response at high loads (Robison et al. 2017).

Collagen cross-links may also contribute to differences in stiffness between the cervix and uterus (Yoshida et al. 2014a). Increased cross-link density and maturity are associated with increasing organ stiffness, therefore, may contribute to greater stiffness identified in the cervix compared to the uterus (Marturano et al. 2013, Eleswarapu et al. 2011, Yoshida et al. 2014a). Transition stretch was significantly larger in the uterus in both the circumferential and axial directions (Fig. 6, $p<0.05$) which may be related to collagen undulation. Prior work showed that collagen undulation in tendons was associated with the toe-region of the stress-stretch curve (Viidik and Ekholm 1968, Viidik 1972, Miller et al. 2012). Therefore, increased transition stretch for the uterus may be due to higher undulation of collagen fibers in the uterus as compared to the cervix. However, differences in collagen undulation between the cervix and uterus in the mouse are currently unknown.

Interestingly, an increase in the *c* parameter in the cervix indicates a less distensible material. This term is assumed to represent the isotropic ground matrix. As expected from studies of the elastin content in the non-pregnant uterus and cervix in mouse (Shimizu and Hokano 1988), rat (Harkness and Moralee 1956, Sharrow et al. 1989), and human models

(Morrione and Seifter 1962, Rorie and Newton 1967), elastin content was not significantly different between locations.

This implies that other components of the ECM, such as proteoglycans or glycosaminoglycans (GAG), may also contribute to the differences in the ground matrix response. GAG content within the uterus is greater in comparison to the cervix in rats (Yao et al. 2014, Fernandez 2013, Simões et al. 2012). Variability within the *c* parameter for the cervix may be related to the ground matrix constituents (Table 3). Decreased microstructural content of the ground matrix within the cervix may alter the accuracy of describing the non-linear response as the neo-Hookean term in research on the vein and carotid artery did not describe the forces within the low strain regime accurately (Sokolis et al. 2011, Sokolis 2013).

Previous studies employed mechanical testing and constitutive modeling on the cervix with varying results (Liao et al. 2014, Myers et al. 2015, Yoshida et al. 2016). Liao *et al.*, described mechanical responses in the human cervix utilizing the three fiber family (3FF) model with a neo-Hookean component (Liao et al. 2014). Our present study utilized a neo-Hookean term to describe the elastic fiber isotropic matrix term, however, the 3FF model for the murine cervix was over-parameterized (Yin et al. 1986). Past studies investigated the uniaxial cervical response through pregnancy utilizing a fibrous composite model for murine and human organs (Myers et al. 2015, Yoshida et al. 2016). Differences between model results may be linked to comparing uniaxial experiments in previous studies to the biaxial experiments performed within this study. Applying the material properties and the 2FF+NH model to a finite element model may provide insights into the

interface of the cervix and uterus leading to improved understanding of pathologies such as cervical insufficiency (Fernandez et al. 2016, Westervelt et al. 2017).

4.1 Limitations

Differences in mechanical properties within the estrous cycle were not considered for this study. A small pilot study (n=6) comparing mechanical properties in estrus and diestrus mice revealed no significant differences in transition stretch (p>0.05), transition stress (p>0.05), toe-modulus (p>0.05), and linear-modulus (p>0.05) for the cervix and uterus, respectively, which is consistent with results from the rat vagina (Moalli et al. 2005). Several studies chose a single point in the estrous cycle for consistency and as a representative of the non-pregnant cervix (Yoshida et al. 2014b, Alperin et al. 2010). Thickness values for 4 samples were a calculated average from the cervix and uterus. The use of an averaged value for the four samples may cause minute changes in the calculation of mechanical properties, however, prior research used averaged thickness values within calculations (Lee et al. 2013).

While 2D frameworks are valuable tools for modeling experimental data (Humphrey 2002, Gleason et al. 2008, Ferruzzi et al. 2013), they remain approximations and make assumptions such as homogenous residual stress through the wall and a thin-walled geometry. More work is needed to characterize physiologic relevant pressures, the multiaxial loading on the uterocervical complex, and investigate the collagen undulation and orientation of the murine reproductive system to improve accuracy of computational models.

4.2 Conclusions

In summary, the biaxial mechanical properties of the non-pregnant murine cervix and uterus were determined with inflation-extension biaxial testing. The cervix was significantly stiffer than the uterus in the axial and circumferential directions. Furthermore, *in vivo* ultrasound measured significant differences in geometry and histological analysis identified microstructural differences with location. Increased stiffness and a larger cervical outer diameter may inform future research modeling the uterocervical complex. The techniques developed herein may be beneficial for future studies examining the changing structure and region-dependent mechanical environment of the female urogenital system such as finite element models for modeling (patho)physiologic processes.

Table 1: Bilinear Fit Parameters

$\boldsymbol{\sigma_\theta \, vs \, \lambda_\theta}$	**Stretch [-]**	**Stress [kPa]**	**Toe-Modulus [kPa]**	**Linear-Modulus [kPa]**
Uterus	1.39±0.05	6.41±0.51	27.3±2.61	2.82E2±18.9
Cervix	1.16±0.02	8.55±1.05	1.28E2±35.0	7.77E2±99.0
p-Value	$p<0.001$	$p>0.05$	$p<0.005$	$p<0.001$
$\boldsymbol{\sigma_z \, vs \, \lambda_\theta}$				
Uterus	1.38±0.04	5.29±0.59	18.3±1.71	94.8±7.43
Cervix	1.15±0.02	5.11±0.57	65.8±17.7	2.79E2±39.6
p-Value	$p<0.001$	$p>0.05$	$p<0.01$	$p<0.001$

Table 2: 2D 2FF+NH SEF Material Parameters of Uterus

Uterus	c [−]	$\mathbf{c_1}$ [kPa]	$\mathbf{c_2}$ [−]	α [°]	RMSE
Sample 1	1.07E-11	4.20	2.64	48.96	0.34
Sample 2	9.52E-12	7.18	6.73	51.01	0.13
Sample 3	7.53E-11	11.29	5.36	41.83	0.21
Sample 4	5.30E-11	18.92	0.03	44.34	0.39
Sample 5	5.93E-10	9.91	1.31	49.52	0.41
Sample 6	1.90E-11	13.86	0.97	34.68	0.30
Sample 7	7.50E-11	2.45	4.99	55.08	0.33
Sample 8	7.74E-13	0.61	3.48	28.83	0.21
Sample 9	9.02E-11	18.33	7.66	52.67	0.20
Sample 10	2.23E-11	10.89	3.68	47.85	0.28
Sample 11	2.34E-11	14.07	1.57	44.64	0.26
Sample 12	1.39E-10	7.84	5.22	47.99	0.25
Sample 13	1.46E-10	9.98	0.51	52.92	0.45
Sample 14	2.24E-14	3.61	1.34	37.80	0.23
Sample 15	9.70E-12	7.47	2.90	50.65	0.27
Mean±SEM	8.45E-11±3.84E-11	9.37±1.41	3.23±0.61	45.92±1.91	0.28±0.02

Table 3: 2D 2FF+NH SEF Material Parameters of Cervix

Cervix	c [−]	$\mathbf{c_1}$ [kPa]	$\mathbf{c_2}$ [−]	α [°]	RMSE
Sample 1	3.00E-10	77.30	29.10	58.00	0.42
Sample 2	23.40	176.50	139.30	63.00	0.36
Sample 3	39.30	19.10	15.80	60.20	0.39
Sample 4	8.78	75.20	30.00	54.70	0.06
Sample 5	2.72E-14	41.40	10.70	54.20	0.31
Sample 6	14.50	3.66	119.70	38.50	0.32
Sample 7	7.03E-14	79.20	19.80	57.50	0.28
Sample 8	1.93E-11	6.38	3.04	42.30	0.25
Sample 9	2.97	43.90	10.90	54.60	0.10
Sample 10	1.52E-10	14.20	11.90	51.10	0.25
Sample 11	7.44E-12	3.49	4.59	43.60	0.11
Sample 12	3.18E-12	28.70	2.36	49.70	0.35
Sample 13	6.55E-11	33.04	7.78	57.59	0.41
Sample 14	2.16E-10	17.05	1.44	48.36	0.39
Sample 15	26.58	0.02	26.17	38.94	0.51
Mean±SEM	7.70±3.24	41.28±11.95	28.84±10.87	51.50±2.00	0.30±0.03

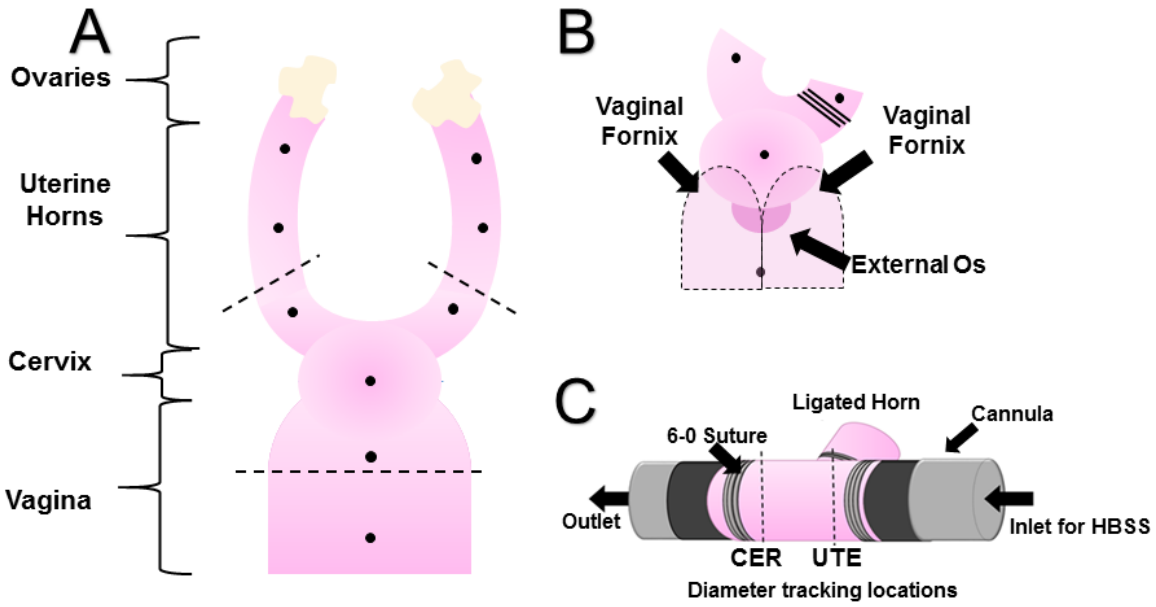

Figure 1: (A) Schematic of the murine female reproductive system with black dots representing the marks made to measure the length of the reproductive tract and dashed lines representing the locations of the singular cuts. (B) Graphic of the utero-cervical complex in preparation for cannulation. The randomly chosen, contralateral uterine horn is ligated and the tissue within dotted outline represents the excess vaginal tissue to be removed to expose the external os. (C) A schematic testing setup of the custom myograph inflation-extension device (Danish MyoTechnologies, Aarhus, Denmark) with utero-cervical complex cannulated in a view from the side. The cervix (CER) and uterine (UTE) body are positioned within the system so that the inlet is connected to the uterine horn and the outlet to the vaginal cervix to mimic the flow from the uterus into the cervix during menstruation or birth.

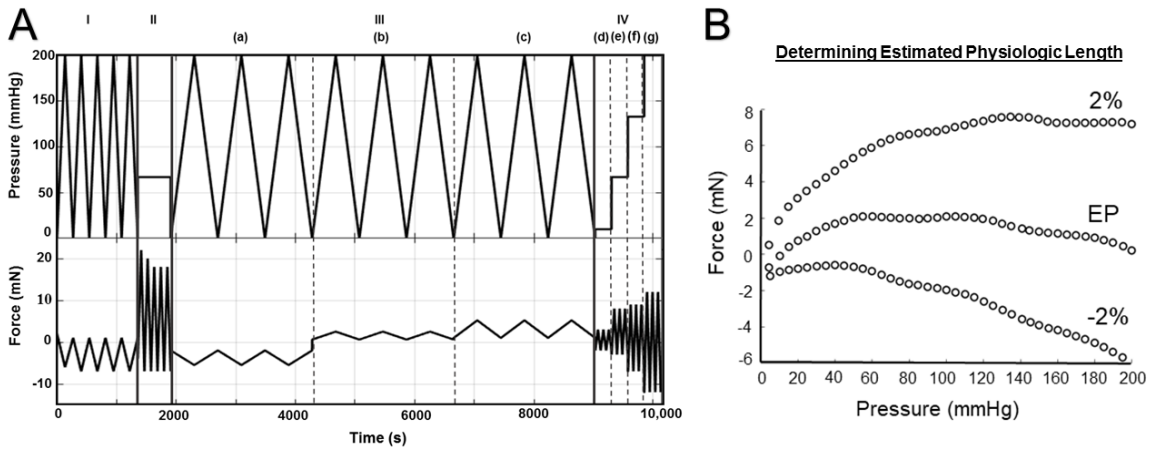

Figure 2: (A) Schematic of the testing protocol demonstrating the changes in pressure and force over time for the different segments of the protocol. The protocol is divided as follows: (I) five cycles of pressure-inflation preconditioning at the unloaded length over the range of physiologic pressures; (II) five force-elongation preconditioning cycles at a constant 1/3 of maximum pressure over a range of stretches up to 10% above the unloaded length; (III) shows three cycles of pressure-inflation at 2% below the estimated physiological (EP) length (a), at the EP length (b), and 2% above the EP length (c); (IV) force-elongation tests with changing stretches from 2% below to 2% above the EP length at constant pressures of 10mmHg (d), 67mmHg (e), 133mmHg (f), and 200mmHg (g). (B) To confirm estimated physiologic (EP) axial stretch, pressure-inflation test data was plotted with axial force against increasing pressure (P=0-200mmHg) from a representative sample at three different stretches (2% below estimated physiologic, estimated physiologic, and 2% above estimated physiologic length).

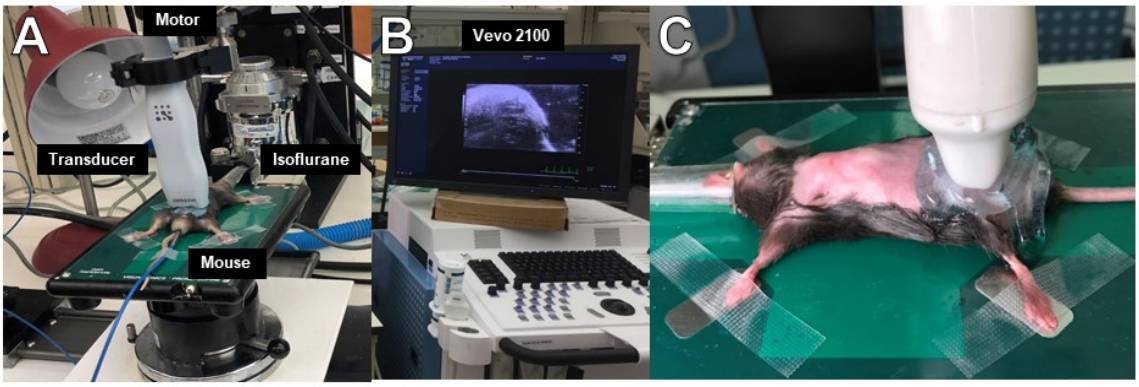

Figure 3: (A) Setup of animal and transducer for reproductive imaging of female C57BL/6 mice using a high frequency ultrasound system. (B) During imaging, vaporized isoflurane gas was administered and both the EKG signal and respiratory rate were monitored. (C) An anesthetized mouse placed on the stage in a supine position with the transducer positioned in the short axis orientation to acquire 3D images of the reproductive tract. Heart rate and EKG were monitored through electrodes on the stage beneath the animal's paws. Additionally, respiratory rate was acquired through low frequency changes in the EKG signal. The ultrasound system acquired 3D scans of the reproductive tract via a linear step motor with a step size of 0.19mm via serial short axis B-mode images averaging approximately 36 slices per reconstruction.

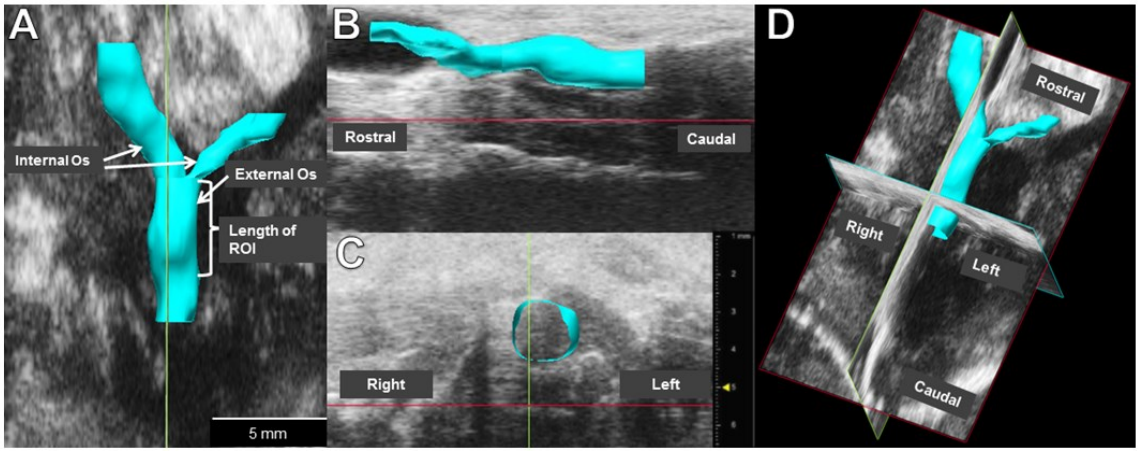

Figure 4: Ultrasound images compiled into 3D segmentations of the reproductive tract exploring the regions of interest (ROI). (A) Coronal view of the murine reproductive tract that extends into the uterine horns and the external os which is located at a transitional region between the cervix and vagina. Length of the ROI was measured from the split of the uterine horns to the edge of vaginal/cervical border region based on gross anatomical descriptions from past work in rodent models c.f. (Leppi 1964). (B) Sagittal view along the length of the murine reproductive system depicting the cervical/vaginal border region transitioning into the right uterine horn. (C) Axial view of murine cervix showing a cross-section at the region above the opening into the vaginal canal. (D) Compiled 3D view along the length of the murine cervix and lower uterine segment.

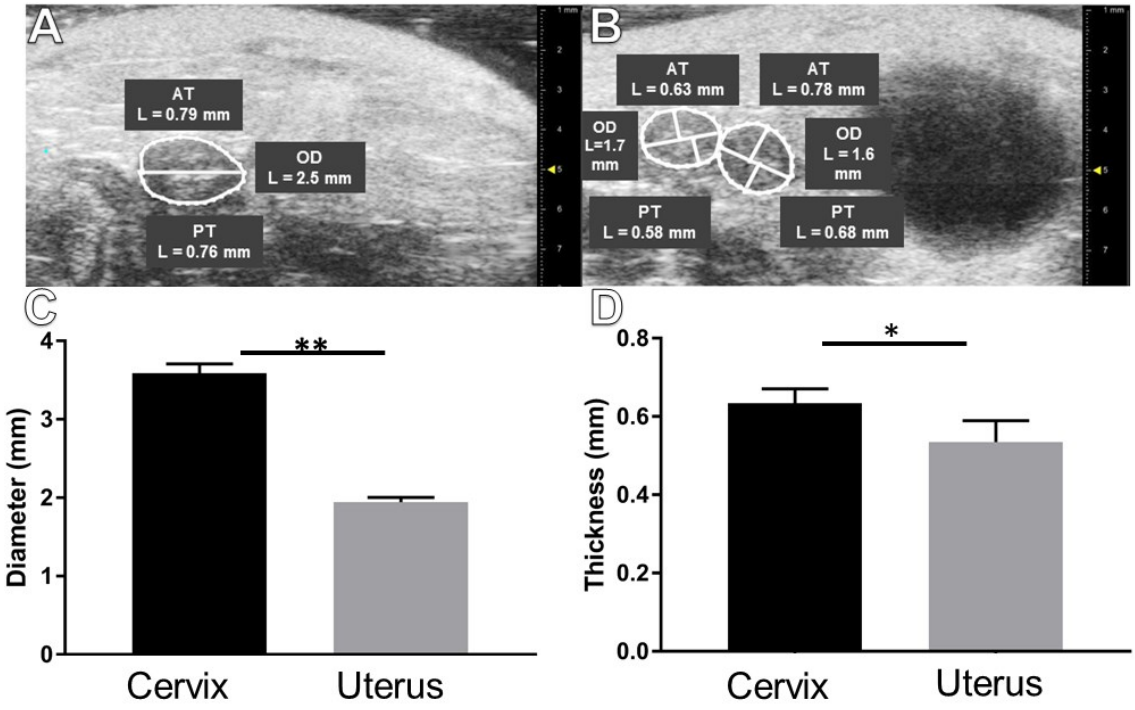

Figure 5: (A), (B) Representative measurements of outer horizontal diameter (OD), anterior thickness (AT), and posterior thickness (PT) taken in the region of the cervix (A) and the uterus (B), where the canal for both uterine horns acts as a location marker for geometric analysis. (C) *In vivo* outer horizontal diameter for the cervix was significantly larger ($p<0.01$**) than the uterus in which cervical diameter was 3.59±0.12mm and uterine diameter 1.95±0.06mm (D) Calculated *in vivo* wall thickness, from averaged anterior and posterior measurements at both locations, was significantly larger within the cervix at 0.63±0.04mm compared to 0.54±0.05mm in the uterus ($p<0.05$*).

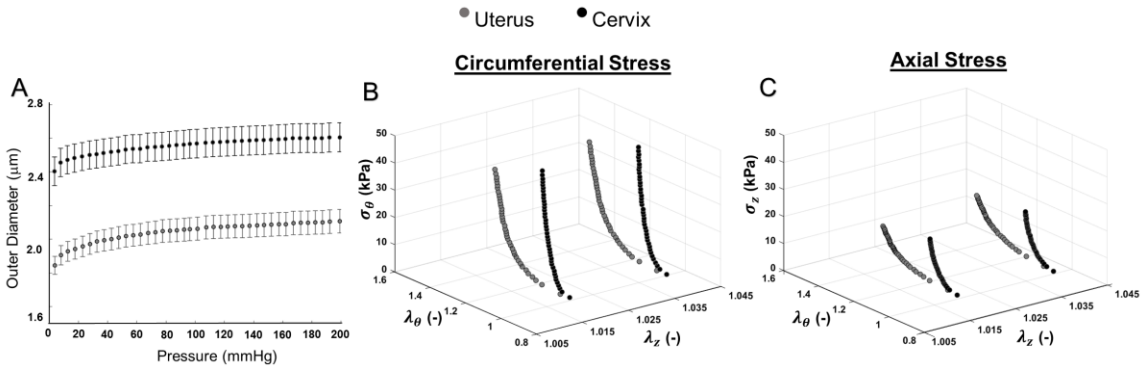

Figure 6: (A) Outer diameter changes with increasing pressure in the cervix (•) and uterus (•) during the pressure-diameter tests. Data shown as mean±SEM (n=12). Representative circumferential (B) and axial (C) Cauchy stress-stretch curves for the cervix (•) and uterus (•) demonstrate the cervix is significantly (p<0.001) less distensible than the uterus with reported circumferential transition stretches of 1.15±0.02 and 1.39±0.05, respectively. Furthermore both organs are stiffer in the circumferential direction compared to the axial with significantly greater circumferential toe- and linear-moduli (Table 1).

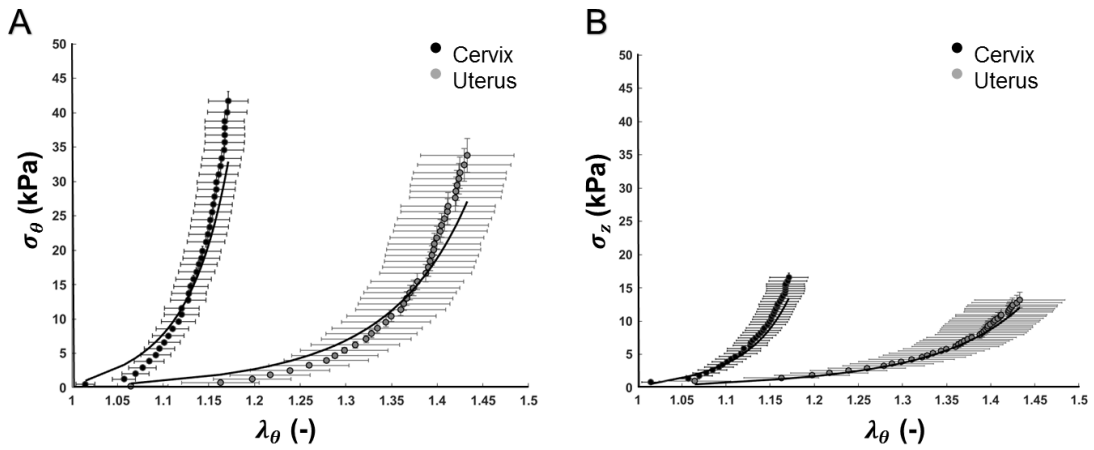

Figure 7: Pressure-diameter tests for cervix (•) and the uterus (•) with model fits (-) (mean±SEM) for the 2D two-fiber family with a neo-Hookean term (2D 2FF+NH) model Cauchy circumferential stress (A) and Cauchy axial stress (B). The neo-Hookean term representing the isotropic ground matrix was significantly larger (p<0.05) in the cervix. Further, both the c_1 stress-like parameter (p<0.01) and the c_2 parameter (p<0.05) representing the symmetric diagonal collagen fibers was significantly higher than the uterus, suggesting that the cervix is less distensible.

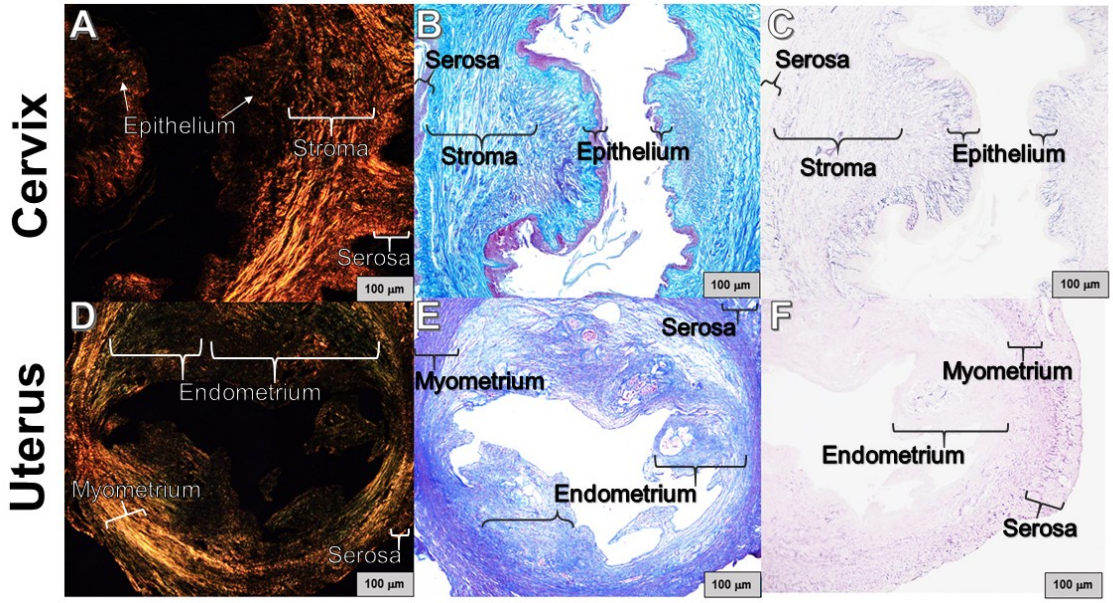

Figure 8: Picrosirius red (PSR) (A, D), Masson's trichrome (MT) (B, E), and Hart's Elastic stain (C, F) images taken at 10x magnification of the cervix (top row) and uterus (bottom row) with labeling for the layers of each organ. The cervix collagen fiber ratio of large diameter to small diameter was approximately 10:1 (A), collagen and smooth muscle content was 75.6±4.49% and 15.7±3.90%, respectively (B), and elastic fiber content was 3.32±0.57% (C). The uterus presented a collagen fiber ratio of approximately 7:1 (D) and collagen (E), smooth muscle (E), and elastic fiber (F) area fractions of 69.6±5.23%, 18.4±1.55%, and 3.63±1.16%, respectively. A significantly greater collagen content ($p<0.005$) and significantly decreased SMC content ($p<0.001$) was identified for the cervix compared to the uterus. No significant differences were identified for elastic fiber content between organs.

ACKNOWLEDGMENTS

The authors wish to thank Katy Robison and Daniel Capone for technical assistance and Mala Mahendroo for support.

FUNDING

This work was supported by the Tulane Newcomb College Institute Faculty Grant (KSM), NSF CMMI 1751050 (KSM), Ochsner Translational Medicine Research Initiative (LRK, LD, and KSM), the Louisiana Board of Regents Support Fund Fellowship (CKC), and the Louisiana Board of Regents (SURE) (VLM).

CONFLICTS OF INTEREST

None to be declared.

References:

Akins, M. L., K. Luby-Phelps, R. A. Bank & M. Mahendroo (2011) Cervical Softening During Pregnancy: Regulated Changes in Collagen Cross-Linking and Composition of Matricellular Proteins in the Mouse. *Biology of Reproduction,* 84**,** 1053-1062.

Alperin, M., A. Feola, L. Meyn, R. Duerr, S. Abramowitch & P. Moalli (2010) Collagen scaffold: a treatment for simulated maternal birth injury in the rat model. *American Journal of Obstetrics and Gynecology,* 202**,** 589.e1-589.e8.

Amin, M., V. P. Le & J. E. Wagenseil (2012) Mechanical Testing of Mouse Carotid Arteries: from Newborn to Adult. *Journal of Visualized Experiments*.

Baah-Dwomoh, A., J. McGuire, T. Tan & R. De Vita (2016) Mechanical Properties of Female Reproductive Organs and Supporting Connective Tissues: A Review of the Current State of Knowledge. *Applied Mechanics Reviews,* 68.

Barnum, C. E., J. L. Fey, S. N. Weiss, G. Barila, A. G. Brown, B. K. Connizzo, S. S. Shetye, M. A. Elovitz & L. J. Soslowsky (2017) Tensile Mechanical Properties and Dynamic Collagen Fiber Re- Alignment of the Murine Cervix are Dramatically Altered Throughout Pregnancy. *Journal of biomechanical engineering,* 139.

Becker, W. R. & R. De Vita (2015) Biaxial mechanical properties of swine uterosacral and cardinal ligaments. *Biomech Model Mechanobiol,* 14**,** 549-60.

Bersi, M., M. Collins, E. Wilson & J. Humphrey (2012) Disparate changes in the mechanical properties of murine carotid arteries and aorta in response to chronic infusion of angiotensin- II. *International Journal of Advances in Engineering Sciences and Applied Mathematics,* 4**,** 228-240.

Bersi, M., J. Ferruzzi, J. Eberth, R. Gleason & J. Humphrey (2014) Consistent Biomechanical Phenotyping of Common Carotid Arteries from Seven Genetic, Pharmacological, and Surgical Mouse Models. *The Journal of the Biomedical Engineering Society,* 42**,** 1207-1223.

Bulletti, C., D. de Ziegler, V. Polli, L. Diotallevi, E. Del Ferro & C. Flamigni (2000) Uterine contractility during the menstrual cycle. *Hum. Reprod.,* 15**,** 81-89.

Byers, S. L., M. V. Wiles, S. L. Dunn & R. A. Taft (2012) Mouse estrous cycle identification tool and images. *PloS one,* 7**,** e35538.

Capone, D. J., G. L. Clark, D. Bivona, B. O. Ogola, L. Desrosiers, L. R. Knoepp, S. H. Lindsey & K. S. Miller (2018) Evaluating residual strain throughout the murine female reproductive system. *Journal of Biomechanics*.

Collins, M., J. Eberth, E. Wilson & J. Humphrey (2012) Acute mechanical effects of elastase on the infrarenal mouse aorta: implications for models of aneurysms. *Journal of biomechanics,* 45**,** 660-665.

Conrad, J. T., W. L. Johnson, W. K. Kuhn & C. A. Hunter (1966) Passive stretch relationships in human uterine muscle. *American Journal of Obstetrics and Gynecology,* 96**,** 1055-1059.

Danforth, D. N. (1947) The fibrous nature of the human cervix, and its relation to the isthmic segment in gravid and nongravid uteri. *American Journal of Obstetrics and Gynecology,* 53**,** 541-560.

Eleswarapu, S. V., A. Almarza, D. J. Responte & K. A. Athanasiou (2011) Tensile Properties, Collagen Content, and Crosslinks in Connective Tissues of the Immature Knee Joint. *PLoS ONE,* 6**,** e26178.

Ferland, D. J., E. S. Darios & S. W. Watts (2015) The persistence of active smooth muscle in the female rat cervix through pregnancy. *Am J Obstet Gynecol,* 212**,** 244.e1-8.

Fernandez, M. (2013) Direct measurement of the permeability of human cervical tissue. *Journal Of Biomechanical Engineering,* 135**,** 021024.

Fernandez, M., M. House, S. Jambawalikar, N. Zork, J. Vink, R. Wapner & K. Myers (2016) Investigating the mechanical function of the cervix during pregnancy using finite element models derived from high-resolution 3D MRI. *Computer Methods in Biomechanics and Biomedical Engineering,* 19**,** 404-417.

Ferruzzi, J., M. Bersi & J. Humphrey (2013) Biomechanical Phenotyping of Central Arteries in Health and Disease: Advantages of and Methods for Murine Models. *Ann Biomed Eng,* 41**,** 1311-1330.

Fung, Y., K. Fronek & P. Patitucci (1979) Pseudoelasticity of arteries and the choice of its mathematical expression. *American Journal of Physiology-Heart and Circulatory Physiology,* 237**,** H620-H631.

Garipcan, B., S. Maenz, T. Pham, U. Settmacher, K. D. Jandt, J. Zanow & J. Bossert (2011) Image Analysis of Endothelial Microstructure and Endothelial Cell Dimensions of Human Arteries – A Preliminary Study. *Advanced Engineering Materials,* 13**,** B54-B57.

Gleason, R. L., W. W. Dye, E. Wilson & J. D. Humphrey (2008) Quantification of the mechanical behavior of carotid arteries from wild-type, dystrophin-deficient, and sarcoglycan- δ knockout mice. *Journal of Biomechanics,* 41**,** 3213-3218.

Gleason, R. L., S. P. Gray, E. Wilson & J. D. Humphrey (2004) A Multiaxial Computer-Controlled Organ Culture and Biomechanical Device for Mouse Carotid Arteries. *Journal of Biomechanical Engineering,* 126**,** 787.

Harkness, M. L. & R. D. Harkness (1959) Changes in the physical properties of the uterine cervix of the rat during pregnancy. *The Journal of physiology,* 148**,** 524.

--- (1961) The mechanical properties of the uterine cervix of the rat during involution after parturition. *The Journal of physiology,* 156**,** 112.

Harkness, R. D. & B. E. Moralee (1956) The time- course and route of loss of collagen from the rat's uterus during post- partum involution. *The Journal of physiology,* 132**,** 502.

Holzapfel, G., T. Gasser & R. Ogden (2000) A New Constitutive Framework for Arterial Wall Mechanics and a Comparative Study of Material Models. *Journal of elasticity and the physical science of solids,* 61**,** 1-48.

Humphrey, J. D. 2002. *Cardiovascular Solid Mechanics Cells Tissues and Organs*. New York: Springer-Verlag New York Inc.

Lake, S. P., K. S. Miller, D. M. Elliott & L. J. Soslowsky (2009) Effect of fiber distribution and realignment on the nonlinear and inhomogeneous mechanical properties of human supraspinatus tendon under longitudinal tensile loading. *Journal of Orthopaedic Research,* 27**,** 1596-1602.

Lee, Y. U., Y. Naito, H. Kurobe, C. K. Breuer & J. D. Humphrey (2013) Biaxial mechanical properties of the inferior vena cava in C57BL/6 and CB-17 SCID/bg mice. *Journal of Biomechanics,* 46**,** 2277-2282.

Lepage, J., C. Jayyosi, P. Lecomte-Grosbras, M. Brieu, C. Duriez, M. Cosson & C. Rubod (2015) Biomechanical pregnant pelvic system model and numerical simulation of childbirth: impact of delivery on the uterosacral ligaments, preliminary results. *International Urogynecology Journal,* 26**,** 497-504.

Leppert, P. C., J. M. Cerreta & I. Mandl (1986) Orientation of elastic fibers in the human cervix. *American journal of obstetrics and gynecology,* 155**,** 219.

Leppert, P. C., S. Y. Yu, S. Keller, J. Cerreta & I. Mandl (1987) Decreased elastic fibers and desmosine content in incompetent cervix. *American journal of obstetrics and gynecology,* 157**,** 1134.

Leppi, T. J. (1964) A study of the uterine cervix of the mouse. *Anatomical Record,* 150**,** 51-65.

Liao, D., L. Hee, P. Sandager, N. Uldbjerg & H. Gregersen (2014) Identification of biomechanical properties in vivo in human uterine cervix. *Journal of the Mechanical Behavior of Biomedical Materials,* 39**,** 27-37.

Loeb, L., V. Suntzeff & E. L. Burns (1938) THE EFFECTS OF AGE AND ESTROGEN ON THE STROMA OF VAGINA, CERVIX AND UTERUS IN THE MOUSE. *Science,* 88**,** 432-3.

Lumsden, M. A. & D. T. Baird (1985) INTRA- UTERINE PRESSURE IN DYSMENORRHEA. *Acta Obstetricia et Gynecologica Scandinavica,* 64**,** 183-186.

Luo, J., L. Chen, D. E. Fenner, J. A. Ashton-Miller & J. O. DeLancey (2015) A multi-compartment 3-D finite element model of rectocele and its interaction with cystocele. *J Biomech,* 48**,** 1580-6.

Manoogian, S. J., C. McNally, J. D. Stitzel & S. M. Duma (2008) Dynamic biaxial tissue properties of pregnant porcine uterine tissue. *Stapp car crash journal,* 52**,** 167.

Marturano, J. E., J. D. Arena, Z. A. Schiller, I. Georgakoudi & C. K. Kuo (2013) Characterization of mechanical and biochemical properties of developing embryonic tendon.(BIOPHYSICS AND COMPUTATIONAL BIOLOGY: ENGINEERING)(Author abstract). *Proceedings of the National Academy of Sciences of the United States,* 110**,** 6370.

Miller, K. S., B. K. Connizzo, E. Feeney & L. J. Soslowsky (2012) Characterizing local collagen fiber re- alignment and crimp behavior throughout mechanical testing in a mature mouse supraspinatus tendon model. *Journal of Biomechanics,* 45**,** 2061-2065.

Milsom, I., B. Andersch & G. Sundell (1988) The Effect Of Flurbiprofen And Naproxen Sodium On Intra- Uterine Pressure And Menstrual Pain In Patients With Primary Dysmenorrhea. *Acta Obstetricia et Gynecologica Scandinavica,* 67**,** 711-716.

Moalli, P. A., N. S. Howden, J. L. Lowder, J. Navarro, K. M. Debes, S. D. Abramowitch & S. L. Woo (2005) A rat model to study the structural properties of the vagina and its supportive tissues. *Am J Obstet Gynecol,* 192**,** 80-8.

Morrione, T. G. & S. Seifter (1962) Alteration in the collagen content of the human uterus during pregnancy and post partum involution. *The Journal of experimental medicine,* 115**,** 357.

Myers, K. M., C. P. Hendon, Y. Gan, W. Yao, K. Yoshida, M. Fernandez, J. Vink & R. J. Wapner (2015) A continuous fiber distribution material model for human cervical tissue. *Journal of Biomechanics,* 48**,** 1533-1540.

Myers, K. M., S. Socrate, A. Paskaleva & M. House (2010) A study of the anisotropy and tension/compression behavior of human cervical tissue. *Journal of biomechanical engineering,* 132**,** 021003.

Pearsall, G. W. & V. L. Roberts (1978) Passive mechanical properties of uterine muscle (myometrium) tested in vitro. *Journal of Biomechanics,* 11**,** 167,173-171,176.

Peña, E., P. Martins, T. Mascarenhas, R. M. Natal Jorge, A. Ferreira, M. Doblaré & B. Calvo (2011) Mechanical characterization of the softening behavior of human vaginal tissue. *J Mech Behav Biomed Mater,* 4**,** 275-83.

Rasband, W. S. 1997-2016. ImageJ. Bethesda, Maryland, USA: U. S. National Institutes of Health.

Robison, K. M., C. K. Conway, L. Desrosiers, L. R. Knoepp & K. S. Miller (2017) Biaxial Mechanical Assessment of the Murine Vaginal Wall Using Extension-Inflation Testing. *Journal of biomechanical engineering,* 139.

Rorie, D. K. & M. Newton (1967) Histologic and chemical studies of the smooth muscle in the human cervix and uterus. *American Journal of Obstetrics and Gynecology,* 99**,** 466-469.

Ruifrok, A. C. & D. A. Johnston (2001) Quantification of histochemical staining by color deconvolution. *Analytical and quantitative cytology and histology,* 23**,** 291.

Sharrow, L., D. Tinker, J. M. Davidson & R. B. Rucker (1989) Accumulation and regulation of elastin in the rat uterus. *Proc Soc Exp Biol Med,* 192**,** 121-6.

Shimizu, K. & M. Hokano (1988) Removal of collagen bundles in murine uterus during postpartum involution. *Anatomical Record,* 220**,** 138-142.

Simões, R. S., R. M. Oliveira-Filho, H. B. Nader & E. C. Baracat (2012) Glycosaminoglycan profiles in the uterus of adult ovariectomized rats treated with estrogen and progestagen. *European Journal of Obstetrics and Gynecology,* 165**,** 265-270.

Sokolis, D., S. Sassani, E. Kritharis & S. Tsangaris (2011) Differential histomechanical response of carotid artery in relation to species and region: mathematical description accounting for elastin and collagen anisotropy. *Medical & Biological Engineering & Computing,* 49**,** 867-879.

Sokolis, D. P. (2013) Experimental investigation and constitutive modeling of the 3D histomechanical properties of vein tissue. *Biomechanics and modeling in mechanobiology,* 12**,** 431-451.

Sparavigna, A. C. (2014) GIMP and Wavelets for Medical Image Processing: Enhancing Images of the Fundus of the Eye. 0.

Van Loon, P. (1976) Length-force and volume-pressure relationships of arteries. *Biorheology,* 14**,** 181-201.

Viidik, A. (1972) Simultaneous mechanical and light microscopic studies of collagen fibers. *Zeitschrift für Anatomie und Entwicklungsgeschichte,* 136**,** 204-212.

Viidik, A. & R. Ekholm (1968) Light and electron microscopic studies of collagen fibers under strain. *Zeitschrift für Anatomie und Entwicklungsgeschichte,* 127**,** 154-164.

Westervelt, A. R., M. Fernandez, M. House, J. Vink, C.-L. Nhan-Chang, R. Wapner & K. M. Myers (2017) A Parameterized Ultrasound-Based Finite Element Analysis of

the Mechanical Environment of Pregnancy. *Journal of biomechanical engineering,* 139.

Yao, W., K. Yoshida, M. Fernandez, J. Vink, R. J. Wapner, C. V. Ananth, M. L. Oyen & K. M. Myers (2014) Measuring the compressive viscoelastic mechanical properties of human cervical tissue using indentation. *Journal of the Mechanical Behavior of Biomedical Materials,* 34**,** 18-26.

Yin, F. C. P., P. H. Chew & S. L. Zeger (1986) An approach to quantification of biaxial tissue stress-strain data. *Journal of Biomechanics,* 19**,** 27-37.

Yoshida, K., H. Jiang, M. Kim, J. Vink, S. Cremers, D. Paik, R. Wapner, M. Mahendroo & K. Myers (2014a) Quantitative evaluation of collagen crosslinks and corresponding tensile mechanical properties in mouse cervical tissue during normal pregnancy. *PloS one,* 9**,** e112391.

Yoshida, K., M. Mahendroo, J. Vink, R. Wapner & K. Myers (2016) Material properties of mouse cervical tissue in normal gestation. *Acta Biomaterialia,* 36**,** 195-209.

Yoshida, K., C. Reeves, J. Vink, J. Kitajewski, R. Wapner, H. Jiang, S. Cremers & K. Myers (2014b) Cervical collagen network remodeling in normal pregnancy and disrupted parturition in Antxr2 deficient mice. *Journal of biomechanical engineering,* 136**,** 021017.